ACS Catalysis

RESEARCH ARTICLE

pubs.acs.org/acscatalysis

Kinetic Modeling of Pt Catalyzed and Computation-Driven Catalyst Discovery for Ethylene Glycol Decomposition

M. Salciccioli and D. G. Vlachos*

Department of Chemical Engineering, Catalysis Center for Energy Innovation and Center for Catalytic Science and Technology, University of Delaware, Newark, Delaware 19716-3110, United States

Supporting Information

ABSTRACT: Knowledge of the underlying mechanisms controlling oxygenate catalytic decomposition to synthesis gas can lead to the design of better catalysts and reactors, enabling the utilization of biomass feedstock for fuels and chemicals. This work studies the decomposition of ethylene glycol, as a simple surrogate to biomass-derived polyols, through the analysis of two catalytic kinetic models. First, a density functional theory (DFT) and statistical mechanical parametrized model of 81 reversible, elementary-like reactions is used to predict and understand ethylene glycol decomposition on Pt. Reaction path analysis indicates that while the majority of decomposition occurs through initial O−H bond breaking, initial C−H bond breaking is active at temperatures around 500 K. Further, sensitivity analysis shows that early dehydrogenation reactions (specifically $HOCH_2CH_2O^* \rightarrow HOCH_2CHO^* + H^*$) are kinetically important reactions, rather than C−C bond breaking. We show that steady state reactor conditions open up new reaction pathways not seen in surface science (temperature programmed desorption) experiments. The second model, parametrized based on semiempirical linear scaling and linear free energy relationships, consists of 250 reversible, elementary-like reactions and maps the dependence of ethylene glycol decomposition rate and selectivity to various products versus atomic binding energy descriptors. The results show that an optimal catalyst that maximizes the H_2 production rate should have binding energies of 58, 116, and 145 kcal/mol for atomic hydrogen, oxygen, and carbon, respectively. These models can be used to guide future experimental efforts in developing catalysts for polyol reforming.

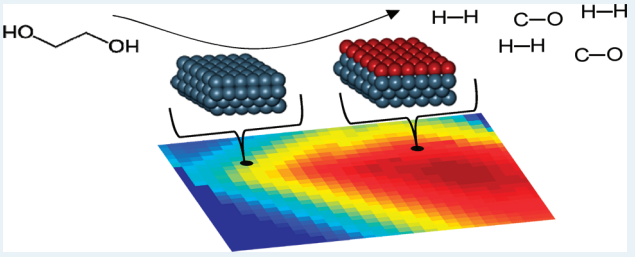

KEYWORDS: ethylene glycol, dehydrogenation, decomposition, Pt, Ni/Pt, rational catalyst design, microkinetic model, linear scaling relationships, Brønsted−Evans−Polanyi relationships, catalysis

1. INTRODUCTION

Understanding the fundamental mechanisms and reaction pathways controlling the transformation of oxygenated hydrocarbons to synthesis gas is central to the utilization of biomass for renewable fuels and chemicals. Biomass-derived synthesis gas allows not only for the production of fuels, chemicals, and electricity via well-established routes,[1] but also for the direct, onsite upgrade of biomass derivatives, without relying on natural gas.[2] Ethylene glycol has emerged as a surrogate for larger biomass derived polyols.[3−11] It is the smallest polyol with a 1:1 ratio of carbon to oxygen (e.g., typical cellulose stoichiometry) and does not require additional steam or oxygen, at least in principle, to remove carbon from the catalytic surface during decomposition

$$C_2H_6O_2 \rightarrow 3H_2 + 2CO \quad (1)$$

Further, ethylene glycol can be obtained with high selectivity from cellulose over a nickel promoted tungsten carbide catalyst.[12,13] Finally, fundamental surface science studies under ultrahigh vacuum (UHV) conditions[5,10,11] and density functional theory (DFT) calculations[6−8] of intermediates and transition states are feasible because of the sufficient vapor pressure and relatively small size of the molecule, respectively.

The elementary reactions involved in decomposition of ethylene glycol (global reaction shown in eq 1) are an important subset of reactions involved in more complex steam reforming, oxidation, or autothermal reforming chemistries.[3] Our recent work has combined DFT and UHV experiments to reveal the reaction pathways of ethylene glycol decomposition on Pt and on the more active Ni/Pt bimetallic catalyst in temperature programmed desorption.[8] The mechanistic insights gained have yet to be applied to computation-based design of catalysts. Catalytic kinetic modeling can assist in bridging the gap between theory and experiments at ideal (single crystal, UHV) conditions and practical reactor conditions.[14,15] Recent advancements in this direction entail detailed DFT based kinetic and thermodynamic parameter calculation[15−19] or semiempirical parameter estimation with metal transferability from a single metal to a number of metals in the periodic table.[7,15,20−23] Such models have provided

Received: July 6, 2011
Revised: August 15, 2011
Published: August 16, 2011

 © 2011 American Chemical Society

unprecedented insights into reaction mechanisms and proven fruitful for catalyst discovery for many smaller chemistry sets.[24−31]

A first attempt at modeling the vapor-phase thermal decomposition of ethylene glycol to synthesis gas on Pt[6] used a reduced model consisting of 7 lumped reactions. The thermodynamic and kinetic parameters of the lumped steps in this model were obtained from a combination of DFT calculations and semiempirical methods. The sensitive parameters of the reduced model were then regressed to supported catalyst experimental data.[6] While this modeling strategy yields a model that can describe a specific set of experimental data and be useful in reactor design, the gained mechanistic insights at the elementary reaction scale are limited. A priori assumptions made in formulating such lumped rate expressions are often incorrect, but are masked by extensive fitting to experimental data.[15,32,33] A detailed microkinetic model is necessary to simulate and analyze surface intermediate concentrations and reaction fluxes to gain insights into the mechanism leading to more active and selective catalysts.[15]

In the first part of this work, we present the first detailed, DFT-based catalytic kinetic model of ethylene glycol decomposition over Pt, consisting of 81 reversible elementary-like reactions. This model is analyzed for prevalent reaction pathways, abundant surface intermediates, and sensitive elementary reactions on H_2 production rate. The later part of this work presents a semiempirically parametrized model, consisting of 250 reversible elementary reactions, which is metal transferrable and uses atomic binding energy descriptors to identify optimal ethylene glycol decomposition catalysts. Combined, the two models offer important information for future efforts in catalyst discovery, as insights yielded here can be used to greatly reduce the number of candidate catalysts being tested experimentally.

2. MODEL DEVELOPMENT

2.1. DFT-Based Thermochemical Properties of Adsorbates. DFT calculations were performed using the SIESTA code.[34,35] Troullier-Martins norm-conserving scalar relativistic pseudopotentials were utilized,[36] with a double-ζ plus polarization (DZP) basis set. An energy shift of 0.01 eV was used to determine the localization radii of the basis functions. A DFT supercell approach implemented the Perdew−Burke−Ernzerhof (PBE) form of the generalized gradient approximation (GGA) functional.[37] A mesh cutoff of 200 Ry was used. The nonspin version of the code was utilized, as it has been previously determined that this does not significantly affect the results for systems involving only Pt metal atoms.[38] A 4 layered, 3 × 3 unit cell was used for all calculations in this study. The surface Monkhorst Pack meshes of 5 × 5 × 1 k-point sampling in the surface Brillouin zone was used in all calculations. The top two layers and the adsorbates were relaxed, while the bottom two layers of Pt were frozen. The procedure for vibrational frequency calculation is outlined in a previous publication.[7]

Temperature dependent thermochemical properties of adsorbates were calculated from the vibrational frequencies using statistical mechanics as described previously.[7] Adsorbed ethylene glycol ($C_2H_6O_2$*) is assumed to be weakly bound and behave as a 2D fluid on the surface. The two vibrational modes corresponding to frustrated translational degrees of freedom in this case are substituted with free translational motion in two orthogonal directions parallel to the surface. All values were corrected for zero-point energy (ZPE) and the PV contribution to Gibbs free energy was neglected.[39] Adsorption configurations for C_2H_xO, C_2H_x, CH_xO, and CH_x species were taken from literature.[38,40,41] Absolute enthalpies of adsorbed surface species were referenced from the heats of formation of the most highly hydrogenated species in each set. For example, all $C_2H_xO_2$ surface species were defined with respect to ethylene glycol in the gas-phase and hydrogen atoms adsorbed on separate slabs. Heats of formation of gas-phase molecules were taken from the NIST database.[42] Additionally, thermochemical properties of transition states reported before[8] are defined in a similar manner using all calculated positive vibrational frequencies. The imaginary mode associated with the negative curvature of the reaction coordinate is treated kinetically in the next section. Calculated thermochemical properties of all adsorbates and transition states on Pt(111) are listed in the Supporting Information.

2.2. DFT-Based Kinetic Model of Ethylene Glycol Decomposition on Pt. A mean field catalytic kinetic model was developed to simulate ethylene glycol decomposition on Pt. All C−H, O−H, and C−C bond cleaving reactions from $C_2H_6O_2$ to CO and H_2 products are included. A complete list of reactions is included in the Supporting Information. Although C−O bond scission is possible on Pt catalysts,[43] recent experimental studies of ethylene glycol decomposition on Pt have shown very low selectivity toward hydrocarbon products.[11] For this reason, C−O bond cleaving reactions are not considered important in this first part of the study (but are accounted for in the second part).

Surface reaction rates are described for each elementary reaction using the following equation:[15]

$$r_i = k_i \prod_{j=1}^{N} C_j^{n_j} \tag{2}$$

Here r_i is the rate of reaction i, k_i is the kinetic rate constant of reaction i, and C_j is the surface concentration of species j, with absolute stoichiometric coefficient n_j in reaction i. The product of C_j is over N reactant species of each reaction only. Each kinetic rate constant is defined from the Gibbs free energy change from reactants to the transition state ($\Delta G^{\ddagger}$):[44]

$$k_i = \frac{k_B T}{h} \exp\left(\frac{\Delta G_i{}^{\ddagger}}{k_B T}\right) \tag{3}$$

In this expression, the factor of $(k_B T)/h$ is derived from a numerical approximation of the partition of the vibrational mode associated with negative curvature of the reaction coordinate.[44] Rate constants of C1 (one carbon) dehydrogenation reactions were taken from a previous published microkinetic model that was tuned to relevant experimental data.[19] Thermodynamic consistency is ensured through the definition of the reverse elementary reaction rate constant (k_b) according to the equilibrium constraint:

$$K_i = \exp\left(\frac{\Delta G_i}{k_B T}\right) = \frac{k_{i,f}}{k_{i,r}} \tag{4}$$

Here, the equilibrium constant (K_i) is a function of the Gibbs free energy of reaction (ΔG_i) and equal to the ratio of the forward and reverse rate constants ($k_{i,f}$ and $k_{i,r}$, respectively).

Ethylene glycol ($C_2H_6O_2$), methanol (CH_3OH), formaldehyde (CH_2O), glycolaldehyde ($HOCH_2CHO$), 1,2 ethenediol (HOCHCHOH), glyoxal (OCHCHO), hydrogen (H_2), and carbon monoxide (CO) were included as gas-phase species.

dx.doi.org/10.1021/cs2003593 |ACS Catal. 2011, 1, 1246–1256

Table 1. Interaction Terms for Microkinetic Model on Pt

adsorbate (*) or transition state (‡)	linear interaction coefficient [kcal/mol]
CO*	$11.5\theta_{CO}$
H*	$5\theta_{CO} + 3\theta_{H}$
$C_2H_xO_2$*	$7\theta_{CO}$
$C_2H_xO_2$*‡	$7\theta_{CO}$

Thermochemical properties of these species were included from literature.[7,42,45] Adsorption of all gas-phase species is assumed to be nonactivated and follows collision theory.[46]

$$k_{i,\,\mathrm{ads}} = S_i\left(\frac{k_B T}{2\pi M_i}\right) \quad (5)$$

In these cases, the rate constant of adsorption ($k_{i,\mathrm{ads}}$) is a function of the sticking coefficient (s_i), the temperature (T), and the molecular mass of the adsorbate (M_i). In this work, the sticking coefficient of all species is assumed to be unity with the exception of CO and H_2, whose values have been set to 0.8 and 0.1, respectively, in accordance with previous research.[47−49]

Adsorbate−adsorbate and adsorbate-transition state interactions were included to better describe the energetics of the system at conditions consistent with steady state supported catalyst reactor experiments. A summary of these parameters is shown in Table 1. The values show the coverage dependence that should be added (destabilization) to the enthalpy of the species listed in the first column, mainly for adsorbed CO that is the dominant surface species on Pt under decomposition conditions (for details of hierarchical mechanism refinement to account for interactions see review ref 15). The CO−CO interaction is derived from the experiments of Yeo et al.[47] This value is the slope of the initial linear regime of the differential heat of adsorption of CO as a function of CO coverage[47] and agrees well with values used in previous computational studies.[19,46] Hydrogen does not significantly affect the enthalpy of other species.[50] The CO−H interaction and H−H interaction are adapted from published research.[19,46] The effect of CO on $C_2H_xO_2$ (x = 5−6) adsorbates and transition states was probed in this study via DFT. The results showed that destabilization of all species and transition states were similar, and this is reflected in Table 1 by having the same interaction for all $C_2H_xO_2$ adsorbates and transition states. Further information on interactions, including plots of this trend, is included in the Supporting Information.

This microkinetic model is employed in an isothermal plug flow reactor (PFR) under conditions described in Section 3.1. No model parameters were adjusted to predict rates or trends seen in the experimental data.

2.3. Atomic Binding Energy Descriptors for Catalyst Design. To probe trends toward active decomposition catalysts for ethylene glycol, we developed a model which uses atomic binding energy descriptors in combination with semiempirical linear free energy relationships to transfer the kinetic model in the previous section to other metals. The methodological procedure is summarized in the schematic in Figure 1. This scheme is adapted from the methods used by Ferrin et al. to study ethanol decomposition on several metals[27] and extended here within microkinetic modeling. Changing the metal on which ethylene glycol decomposition occurs can affect the selectivity to synthesis gas products. For this reason, in this model, the mechanism is

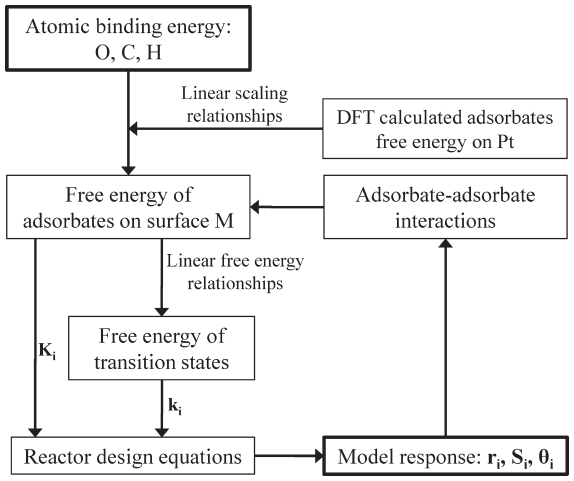

Figure 1. Schematic of kinetic parameter generation for a model based on atomic binding energy descriptors. Here r, S, and θ stand for reaction rate, selectivity, and surface coverage.

expanded to include not only C−H, O−H, and C−C bond cleaving reactions but also C−O bond cleaving reactions and products. Additional gas-phase species for this model include carbon dioxide (CO_2), oxygen (O_2), water (H_2O), ethanol (C_2H_5OH), acetaldehyde (CH_3CHO), ethane (C_2H_6), ethylene (C_2H_4), and methane (CH_4). Thermochemical properties of adsorbed monoalcohol and hydrocarbon fragments and products were calculated on Pt(111) for this purpose and are included in the Supporting Information, along with a full list of reactions for this model.

Atomic binding energies are used to transfer DFT calculated free energies of adsorbates from Pt to a surface/metal of interest via linear scaling relationships.[20−22] We include the transfer of weak binding alcohol (−OH) groups, which enhances the accuracy of these relationships for $C_2H_xO_2$ intermediates.[7] The free energy of adsorbates on the surface of interest are transformed to free energies of activation based on linear free energy (BEP) relationships either developed in this work or found in literature. The relationships developed in this work were regressed from DFT data presented in our previous study[8] and are plotted in the Supporting Information. A summary of the relationships used for each reaction type is included in Table 2. The Gibbs free energies of adsorbates and transition states are next used to compute equilibrium and kinetic rate constants for the entire reaction mechanism. The microkinetic model is then employed in reactor design equations to compute the rate of production of individual species (r_i), the selectivity toward certain products (S_i), and the surface coverages (θ_i), as a function of reactor operating conditions. An important realization is that as the model behavior/response changes with varying atomic binding energies, so do the coverages. This means that it is necessary to expand the inclusion of adsorbate−adsorbate interactions, beyond those of Pt shown in Table 1, to qualitatively reflect these surfaces.

While it is clear that such interaction models should be included in single metal microkinetic models to retain important information on abundant surface adsorbates and rate controlling steps,[17,54] the inclusion of adsorbate−adsorbate interactions in semiempirical models parametrized from atomic binding energy descriptors is a topic still in development. Grabow et al. showed

Table 2. Definition of Linear Free Energy Relationships Used for Each Type of Reaction in Model[a]

reaction description	free energy relationship [kcal/mol]	ref
adsorption/desorption	non activated adsorption	
dehydrogenation of C_xH_y species and β-hydrogen elimination of C_2H_xO species	$\Delta G^{\ddagger} = 1.06\Delta G_{rxn} + 23.1$	38
α-hydrogen elimination of $C_xH_yO_z$ species	$E_{TS} = 1.11E_{FS} + 27.8$	this work
all O−H bond cleavage reactions	$E_{TS} = 0.97E_{FS} + 6.3$	this work
C−C bond cleavage of $C_2H_xO_2$ species	$E_{TS} = 0.87E_{FS} + 24.1$	this work
all C−O bond cleavage	$E_{TS,diss} = 0.87\Delta E_{diss} + 42.9$	51
C−C bond cleavage of C_2H_xO species	$E_{TS} = 0.90E_{FS} + 20.9$	52
C−C bond cleavage of C_2H_x species	$E_{TS} = 0.99E_{FS} + 43.3$	38
CO oxidation to CO_2	$\Delta G^{\ddagger} = 0.74\Delta G_{rxn} + 17.7$	53
C−C bond cleavage for oxygenates with stable gas-phase analogs	$\Delta G^{\ddagger} = 0.78\Delta G_{rxn} + 52.7$	this work

[a] E_{TS} and E_{FS} are energies of the transition states and final states, respectively, referenced from the free energy of the gas-phase analogs of reactant species.[40] $E_{TS,diss}$ and ΔE_{diss} are energies of transition states and final states, respectively, referenced from the free energy of stable gas-phase species (CH_4, H_2O, and H_2).

Table 3. Expanded Model of Adsorbate-Adsorbate Interaction Parameters for Various Surfaces Using Parameters on Pt

species	linear interaction term [kcal/mol]
C*	$50\theta_C + 50\theta_{OHC}$
O*	$16\theta_O$
H*	$3\theta_H + 5\theta_{CO} + 3\theta_{OHC}$
CO*	$11.5\theta_{CO} + 8\theta_{OHC}$
OHC_i*[a]	$50(Q_{i_{pt}}/Q_{C_{pt}})\theta_{OHC} + 8\theta_{CO}$

[a] OHC corresponds to all surface species in the model excluding CO*, H_2O*, OH*, O* and H*. Interaction parameters of these species are estimated from their binding energy and the interaction of C*-C*.

that for a model of the CO oxidation reaction, omission of adsorbate−adsorbate interactions did not change the predicted location of the maximum in activity.[55] On the other hand, they also find that omission of these interaction models greatly affects the shape of the volcano curve.[55] Recent work by Ulissi et al. has shown that inclusion of adsorbate−adsorbate interactions in an atomic binding energy descriptor based model for ammonia decomposition does shift the predicted maximum activity substantially.[31] For more complex chemistry sets (such as ethylene glycol decomposition in this present work), where selective pathways play a role in overall activity, omission of adsorbate−adsorbate interactions will result in the unphysical poisoning and subsequent "shut down" of catalyst surfaces with corresponding atomic binding energies that, in reality, may show significant decomposition activity. This is especially prevalent as C−O bond breaking chemistry becomes active, as previous work has shown the importance of adsorbate−adsorbate interactions in reducing the coverage of hydrocarbon fragments on Pt catalyst surfaces at low temperatures.[56,57] For this reason, we choose to include an approximate model for adsorbate−adsorbate interactions, which is described in the subsequent paragraphs, rather than omitting interactions altogether.

Table 3 summarizes the interaction parameters used in this semiempirical based model. Oxygen formation is plausible for conditions which favor C−O bond cleaving over C−C bond cleaving. The oxygen−oxygen interaction parameter was taken from a previous microkinetic model.[46] In general, calculating interaction parameters of every possible adsorbate−adsorbate combination (even in the simplest case of pairwise additive interactions) is a combinatorial problem. Essentially, with these many adsorbates, calculating all pair interactions would be computationally intractable. For this reason, we implement a general correlation which describes the interactions between alcohol, polyol, and hydrocarbon fragments. This relationship assumes that all alcohol, polyol, and hydrocarbon fragments affect an adsorbate equally. Additionally, the effect of the coverage of these fragments on a species of interest is approximated as proportional to the C−C interaction multiplied by the ratio of the adsorbate binding energy to the atomic carbon binding energy. Although this relationship is qualitative in nature, its implementation does not greatly impact the model results for identifying atomic binding energies that maximize hydrogen production. Metals with high coverages of alcohol or hydrocarbon fragments are most likely not ideal for active and selective decomposition to syngas.

Further, these interaction energies must be adjusted for each new surface/metal modeled. The only information the model has at each new surface is the atomic binding energies and adsorbate thermochemistry and binding energies, which disallows the use of more extensive interaction energy models.[58,59] On the basis of extensive adsorbate−adsorbate interaction calculations over several surfaces,[50] a general trend has been observed whereby interaction energies within metal groups correlate with the absolute binding energy of an adsorbate (see graph in the Supporting Information). For the purposes of this model, this type of relationship is used to "transfer", that is, to predict, the interaction energies on other metals from those on Pt:

$$\omega_{ij}^{M} = \frac{Q_M^{i,0}}{Q_{Pt}^{i,0}}\omega_{ij}^{Pt} \quad (6)$$

where the coverage effect of species j on the energy of species i on metal M (ω_{ij}^{M}) equals this parameter on Pt times the ratio of the zero-coverage binding energies of species i, $Q^{i,0}$, on metal M to Pt. The binding energy of species i on metal M is predicted from the atomic binding energies (C, O, H) on metal M compared to Pt and the binding energy of species i on Pt via linear scaling relationships (see 15). While this adsorbate−adsorbate interaction model is not as accurate as previously reported adsorbate−adsorbate interaction models,[58,59] it allows for the general inclusion of interactions based only on the descriptors governing

dx.doi.org/10.1021/cs2003593 |ACS Catal. 2011, 1, 1246–1256

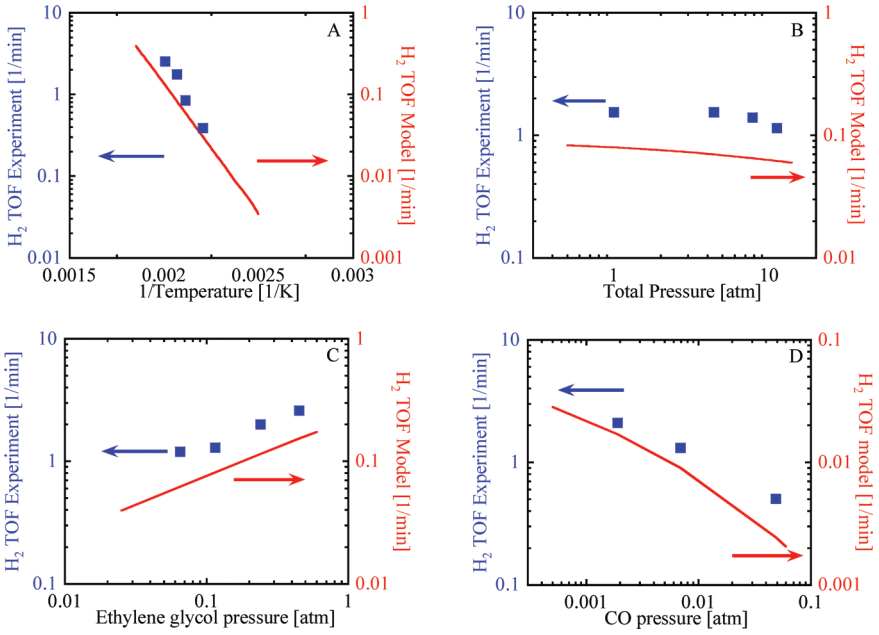

Figure 2. Comparison of kinetic model of this work (red; right vertical axis) to published experimental data of Kandoi et al.[6] (blue; left vertical axis) demonstrating the effect of temperature (A), total pressure (B), ethylene glycol partial pressure (C), and carbon monoxide partial pressure (D) on hydrogen production turnover rate.

the microkinetic model. It is also clear that the inclusion of these (rather rough) interactions is important to the overall findings, as opposed to omitting them completely, as our previous work on NH_3 decomposition has demonstrated.[31] However, it is also important to reiterate that interactions from one metal cannot be transferred to another metal with quantitative accuracy without more advanced models, such as those described by Kitchin and co-workers.[58,59]

The design equation for an isothermal continuously stirred tank reactor (CSTR) was applied to this microkinetic model for numerical convenience. More information on reactor conditions and results are described in Section 4.

3. KINETICS OF ETHYLENE GLYCOL DECOMPOSITION ON PT

The results in Section 3 pertain exclusively to the DFT and statistical mechanical parametrized model described in Section 2.2.

3.1. Prediction of Experimental Trends. The DFT based microkinetic model was compared to recently published kinetically limited experimental data[6] to test how the model captures kinetic trends. The experimental work focused mainly on steam and aqueous phase reforming of ethylene glycol on Pt. There are four sets of experimental data in which no water was added as a reactant.[6] These data sets are compared in Figure 2 (in blue) with the model predictions of this work (in red). The reactor and operating conditions simulated via the microkinetic model match closely those reported in the experimental study.[6]

The simulated $^1/_4$ in. diameter, 1 cm long reactor contained 1.2×10^{19} Pt catalyst sites. The volumetric flow into the reactor used at all conditions was 3.8 cm^3/s (STP). The feeds consisted of a 0.11 molar fraction ethylene glycol and the balance inert nitrogen. The pressure, $C_2H_6O_2$, and CO order simulations were conducted at 483 K and 1 atm. The CO order simulations consisted of a constant $C_2H_6O_2$ feed fraction of 0.06 mol fraction with CO mole fraction varying as specified in Figure 2D.

Table 4. Summary of Intrinsic Kinetic Trends in Pt Model and Experimental Data

metric	model	experiment[6]
apparent activation energy [kcal/mol]	13.6	19.3
total pressure order	−0.26	−0.10
ethylene glycol order	0.38	0.42
carbon monoxide order	−0.54	−0.44

In general, the model predicts hydrogen production rates of about an order of magnitude lower than the experimental data. The overall agreement is remarkably good for this level of chemical complexity given that the DFT and statistical mechanical parameters of the model are unadjusted. Given the coarse-graining involved in going from spatially resolved adsorbates on specific sites to the current mesoscale, mean-field microkinetic model, the lack of describing support effects, the error in the DFT calculations, and the error in the experimental analytical methods, this is a reasonable departure in absolute rates. The more important metric for how the model performs is the ability to describe intrinsic kinetic orders of reactants, temperature, pressure, and inhibiting products.[15] These data are described in Figure 2 and summarized in Table 4. Given the reasonable agreement in reaction order and temperature dependence, only minor adjustments to kinetic parameters would be necessary to quantitatively predict experimental data and use the model for reactor design.

The model shows that the most abundant surface intermediates (MASI) throughout all conditions shown in Figure 2 are H* and CO*. This agrees with the experimental observation by Dumesic and co-workers where attenuated total reflectance infrared (ATR-IR) spectroscopy was used to measure the

dx.doi.org/10.1021/cs2003593 |ACS Catal. 2011, 1, 1246–1256

coverage of CO* during methanol reforming experiments over a Pt catalyst. While ethylene glycol decomposition is kinetically different from methanol steam reforming, these experiments can offer insight into the magnitude of product inhibition on hydrogen production from small oxygenates. Those experiments determined that CO* was present to 55−60% of saturation coverage at 423 K.[60] Additionally, they observed a negative reaction order with respect to hydrogen, suggesting inhibition because of blocking of surface sites by adsorbed hydrogen.[60] The present model shows that CO* coverages are higher at lower temperatures, around 0.5 at 400 K and 1 atm for typical ethylene glycol feeds, and decrease with increasing temperature (see Figure 3). The model shows that the coverage of hydrogen is dictated by the number of sites not occupied by CO*, which is a general observation of the aforementioned experimental work.[60] Further, as the partial pressure of CO is increased, blocking of sites becomes more pronounced (Figure 2D and Figure 3B).

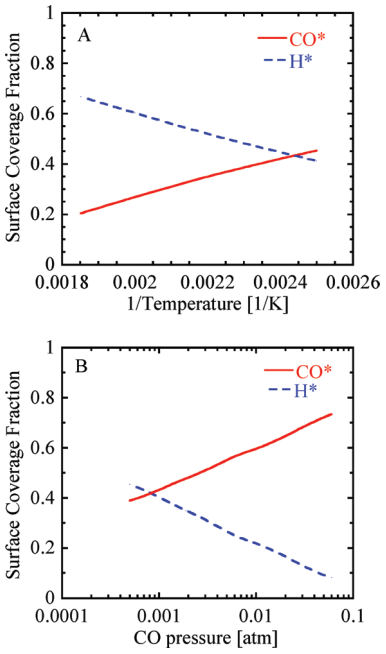

Figure 3. Coverage of most abundant surface intermediates (H* and CO*) as a function of (A) temperature for simulation representing Figure 2A, and (B) CO partial pressure for simulation representing Figure 2D.

While an increase in ethylene glycol pressure has a positive effect on the rate (Figure 2C), there are competing effects due to increased partial pressures of CO and H_2 at the same conversion (Figure 2C and D). Site blocking from products prevails, resulting in negative order with total pressure (Figure 2B).

Aside from predicting experimental trends, a microkinetic model can offer insights into fluxes through specific surface species and elementary reactions that cannot be easily observed or measured experimentally. The next section includes analysis of elementary reaction rates and trends which can offer invaluable insights into the design of improved catalysts and reactors.

3.2. Analysis of Elementary Reaction Contributions. Previous experimental and theoretical studies[7−11,61,62] have focused on low temperature, transient systems. A better understanding of the important pathways at practical application temperatures (∼500 K) and at steady-state can reveal important insights. Analysis of reaction fluxes in kinetic models allows us to understand the specific sequence of bond breaking and forming events, as well as the importance of each elementary reaction.[15]

Figure 4 illustrates the predominant reaction pathways from ethylene glycol to C1 adsorbates under the conditions simulated in Figure 2. The dehydrogenation of C1 adsorbates to syngas on Pt has been described in detail in literature.[11,19,41,63,64] Upon adsorption of ethylene glycol, high barriers to initial C−C bond breaking lead to two viable pathways for decomposition, through initial C−H or O−H bond cleaving.[8] While the dominant path predicted using only DFT-based barriers (no microkinetic modeling) and verified via TPD consists of initial O−H bond cleaving,[8] at steady-state and higher temperatures studied herein, C−H bond cleaving is competitive (Figure 4A). The calculated Gibbs free energy of each intermediate and transition state shown in Figure 4 is illustrated in Figure 5 relative to gas-phase ethylene glycol at 450 K. The inset of Figure 5 compares the calculated Gibbs free energy of activation of initial C−H and O−H bond breaking reactions as a function of temperature. It is apparent that as the temperature increases, the free energy barrier to C−H bond cleaving becomes closer to that of the O−H bond cleaving. This is reflected in Figure 4A where the percentage of ethylene glycol that breaks down through initial C−H cleavage

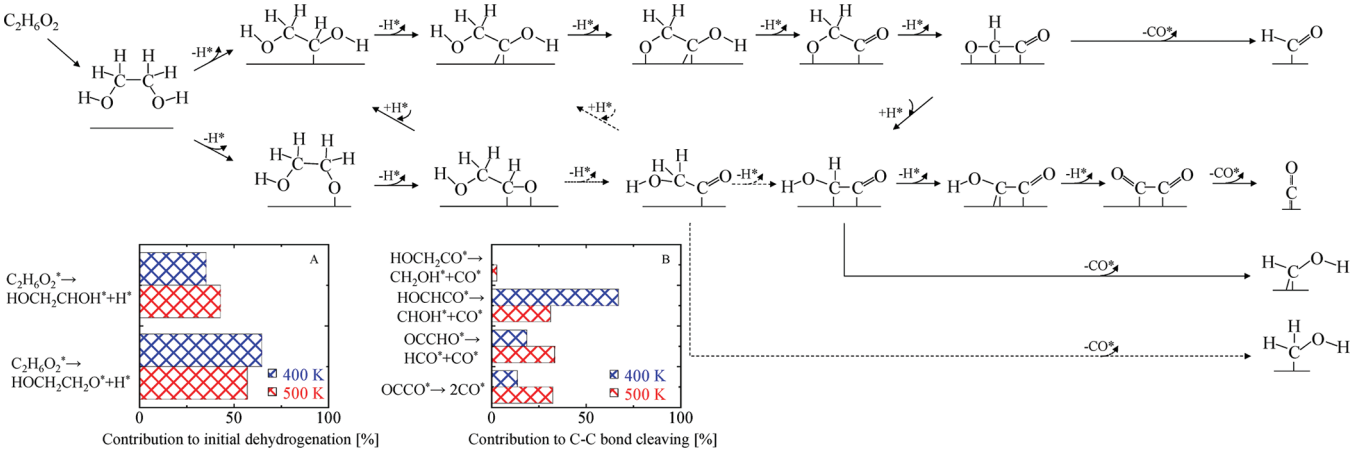

Figure 4. Schematic of major reaction paths of ethylene glycol decomposition on Pt. Minor pathway through $HOCH_2CO$ is shown with dotted arrows. Insets show (A) the percentage of net decomposition occurring through initial C−H and O−H bond breaking and (B) the percentage of net decomposition occurring through four major C−C bond cleaving reactions at 400 and 500 K.

dx.doi.org/10.1021/cs2003593 |ACS Catal. 2011, 1, 1246–1256

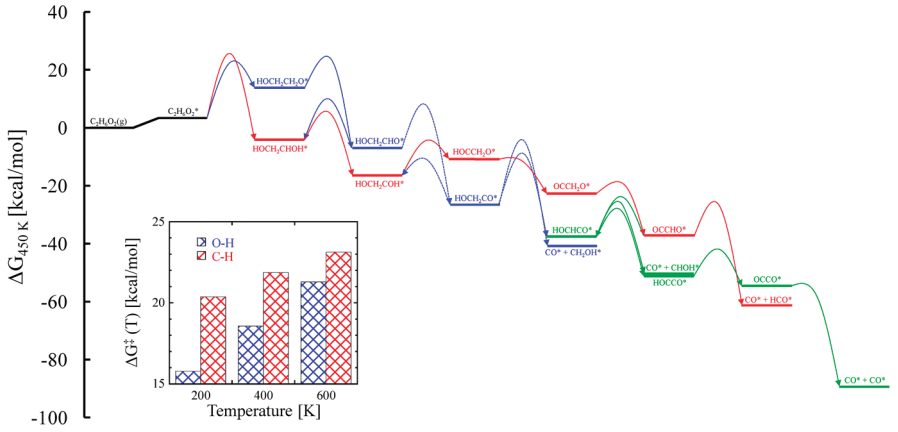

Figure 5. Predicted DFT Gibbs free energy diagram of each adsorbate and transition state relative to gas-phase ethylene glycol and adsorbed hydrogen in the reaction pathways shown in Figure 4 at 450 K in the limit of zero coverage. The inset shows the Gibbs free energy of activation of initial C−H and O−H bond cleaving reactions at three different temperatures. Excess adsorbed hydrogen atoms are omitted for clarity.

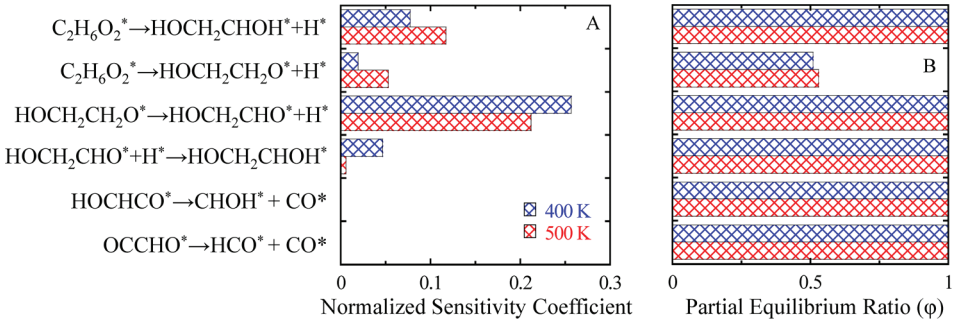

Figure 6. Bar graphs showing (A) normalized sensitivity coefficients and (B) partial equilibrium ratios for select reactions.

draws closer to that of O−H cleavage as the temperature increases.

Further, the pathway through initial O−H cleavage is hindered by another large barrier for glycolaldehyde formation from the alkoxide species. Partial equilibrium analysis shows that this second large barrier causes the reverse reaction of the initial O−H bond pathway to be active (partial equilibrium analysis is the measurement of the reversibility of a reaction calculated through eq 7[32])

$$\phi_i = \frac{r_{f,i}}{r_{f,i} + r_{r,i}} \tag{7}$$

This is the (normalized) ratio of the forward reaction rate to the sum of the forward and reverse rates. A ratio of around 0.5 describes a reaction where the forward and reverse rates are similar, whereas a ratio of 1 or 0 describes an irreversible reaction. The partial equilibrium ratios of several key reactions are shown in Figure 6B. The significant flux through the reverse reaction of the O−H path means the net rate through the initial O−H pathway is much lower than predicted from eqs 2 and 3 alone. This allows the initial C−H breakage to significantly contribute to the ethylene glycol decomposition (Figure 4A).

Following the initial C−H cleavage, subsequent decomposition reactions entail C−C cleavage through the OCCHO* or HOCHCO* surface intermediates. The HOCHCO* forms from surface hydrogenation of the OCCHO* intermediate. This is an interesting dynamic that is not observed in TPD studies. As discussed in a previous publication,[8] because of the decomposition of ethylene glycol happening at or above the desorption temperature of hydrogen, the surface has a very low coverage of hydrogen. In a steady-state reactor at higher temperatures, high coverages of H* because of partial pressure buildup (Figure 3) allow for hydrogenation reactions facilitating decomposition through lower energy paths.

These hydrogenation reactions contribute to the major pathway through initial O−H bond cleavage. Upon formation of glycolaldehyde (after O−H followed by C−H bond cleavage), further decomposition can happen through one of two pathways. Hydrogenation to $HOCH_2CHOH^*$ is favored at lower temperatures with high concentrations of H* and low concentration of vacant surface sites. This pathway merges with the initial C−H pathway (shown in red in Figure 5). At higher temperatures, the pathway through $HOCH_2CO^*$ becomes significant (~40% at 500 K). This intermediate can either hydrogenate to $HOCH_2COH^*$, decompose through C−C cleavage to form hydroxymethyl (CH_2OH^*) and CO*, or continue dehydrogenation to HOCHCO* (entering green path in Figure 5).

Ultimately, a C−C bond scission event is required to transform a $C_2H_xO_2^*$ intermediate into two CH_xO^* intermediates and eventually CO*. Inset (B) in Figure 4 shows the percentage of C−C bond breaking that occurs through $HOCH_2CO^*$, HOCHCO*, OCCHO*, and OCCO*. The most active path for C−C bond cleavage at 400 K is through the HOCHCO* intermediate. As the temperature increases, the pathways through OCCHO* and OCCO* become equally contributing to that of HOCHCO*. C−C cleavage

dx.doi.org/10.1021/cs2003593 |ACS Catal. 2011, 1, 1246–1256

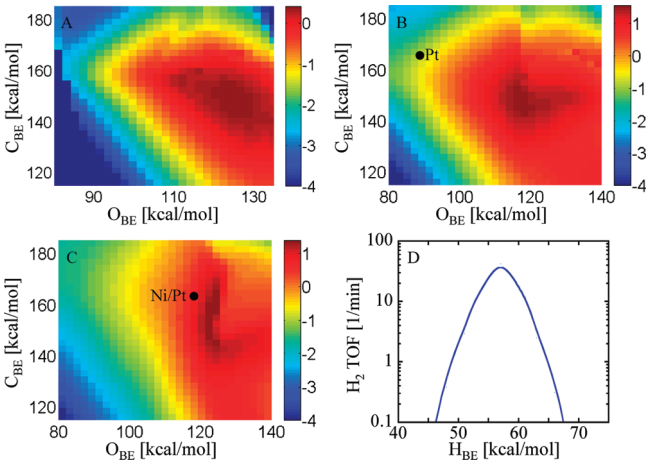

Figure 7. Plots of predicted hydrogen TOF [1/min] (contour plots show log(H_2 TOF)) from ethylene glycol decomposition as a function of C and O atomic binding energies at atomic hydrogen binding energies of (A) 50 kcal/mol, (B) 56 kcal/mol, and (C) 62 kcal/mol. Panel (D) shows the hydrogen production rate as a function of the H binding energy for O_{BE} and C_{BE} fixed to 116 and 146 kcal/mol, respectively. Pt and Ni/Pt labels are put on panels with closest H_{BE}. See Table 5 for actual atomic binding energies and predicted rates of these surfaces.

of $HOCH_2CO^*$ is minor and does not contribute significantly until 500 K.

In the early 1980s, Rabitz and co-workers used local sensitivity analysis on rate constants using first-order finite differences to determine the ranking of the most important reactions in a reaction network.[65−68] This concept was later formalized by Campbell to determine the rate controlling reactions in catalytic systems.[69,70] Similar analysis was carried out to better understand the importance of C−C bond cleaving reactions compared to initial dehydrogenation reactions. This analysis is governed by eq 8

$$\mathrm{NSC}_i = \frac{\mathrm{d}(\ln R_{H_2})}{\mathrm{d}(\ln k_{f,i})} \cong \frac{k_{f,i}\Delta R_{H_2}}{R_{H_2}\Delta k_{f,i}} \quad (8)$$

where the normalized sensitivity coefficient (NSC_i) of each elementary reaction is measured through the change in response of H_2 TOF, R_{H_2}, as a function of the perturbation of each forward rate constant ($k_{f,i}$). Results of selected reactions are shown in Figure 6A. Only initial dehydrogenation reactions show an appreciable effect (the only exception being the hydrogenation of $HOCH_2CHO^*$ to $HOCH_2CHOH^*$ with a minor sensitivity at 400 K). All other reactions, including C−C bond cleaving reactions (two of which are shown in Figure 6A), have negligible normalized sensitivity coefficients for hydrogen production. This analysis is consistent with previous fundamental studies of ethylene glycol decomposition[8,10] and supported catalyst experimental studies of ethylene glycol reforming[71,72] that have speculated that the rate determining step of ethylene glycol decomposition on Pt is not C−C bond breaking. The conversion of the alkoxide ($HOCH_2CH_2O^*$) to the glycolaldehyde mostly controls the overall production of hydrogen (along with some dependence on the initial O−H activation) along the major reaction pathway through initial O−H bond breaking. The other major pathway through initial C−H bond breaking is dependent on the rate of the initial activation of the C−H bond to form the $HOCH_2CHOH^*$ intermediate from ethylene glycol. These rate

Table 5. Atomic Binding Energies and Predicted Hydrogen Production Rates of Discussed Surfaces[a]

	Pt(111)	Ni/Pt(111)	optimal catalyst
C_{BE} [kcal/mol]	165.0	161.6	146.0
O_{BE} [kcal/mol]	89.8	119.0	116.0
H_{BE} [kcal/mol]	56.1	60.8	58.0
H_2 TOF [1/min]	0.2	16.0	36.9

[a] Atomic binding energies are not corrected for ZPE. Hydrogen production rates are shown at identical reactor simulation conditions as in Figure 7.

controlling steps differentiate polyol decomposition from hydrocarbon decomposition where C−C bond cleaving reactions are considered to be rate determining.[56,57]

Understanding the abundant surface species, the reaction pathways, and the sensitive elementary reactions can be important from a mechanistic viewpoint and for reactor optimization. Use of this information, to computationally screen higher performing catalysts, adds another dimension to the value of microkinetic modeling.[15] The next section discusses the implications of the kinetic model on Pt on catalyst design, as well as the results of the semiempirical based model formulated to search for better ethylene glycol decomposition catalysts.

4. COMPUTATIONAL SCREENING FOR ACTIVE ETHYLENE GLYCOL DECOMPOSITION CATALYSTS

Coupling the above analysis with a semiempirical based model, dependent on atomic binding energy descriptors, can give specific targets when seeking better polyol reforming catalysts. Contour plots of predicted H_2 production from ethylene glycol decomposition as a function of C, O, and H atomic binding energies (C_{BE}, O_{BE}, H_{BE}) are shown in Figure 7. These calculations are based on the semiempirical parametrized model discussed in section 2.3. The CSTR reactor simulated is of identical surface area per unit volume as in the previous section, and is operated at 483 K, 1 atm and of feed composition and flow rate equal to that used in Figure 2A. The only difference is that the number of catalyst sites was reduced by a factor of 10, to maintain kinetically relevant conditions.

Labeled in Figure 7 are the binding energies on Pt(111) and those of the experimentally validated more active surface-segregated Ni−Pt−Pt(111) bimetallic catalyst[8,10] (binding energy values and predicted hydrogen production rates are shown in Table 5). It is seen that the major improvement in hydrogen production from the Ni/Pt catalyst compared to the Pt catalyst traces to an increase in atomic oxygen binding energy. This increase in oxygen binding energy increases the rate of the initial dehydrogenation reactions (which have the most control over the hydrogen production on Pt). This increase is the result of many factors indicated from the semiempirically parametrized model (see below).

On the basis of extension of the linear scaling relationships of Nørskov and co-workers[20−22] to complex oxygenates,[7] the free energy of every surface intermediate bound to the surface through an oxygen−metal bond will decrease (stabilize) as the binding energy of atomic oxygen increases (free energy decreases). The dependency varies with the type and number of these oxygen−metal interactions in an intermediate.[7] Importantly, as the binding energy of oxygen increases, the adsorbed

dx.doi.org/10.1021/cs2003593 |ACS Catal. 2011, 1, 1246–1256

ethylene glycol ($HOCH_2CH_2OH^*$) stabilizes slightly based on the interactions of the two hydroxyl groups with the metal. This enhanced stabilization results in an increased flux of ethylene glycol to the surface and an increased concentration of $HOCH_2CH_2OH^*$. Equation 2 dictates that rates of early dehydrogenation reactions increase as the concentration of $HOCH_2CH_2OH^*$ increases. Additionally, species with a strong dependence on the atomic binding energy of oxygen, namely, $HOCH_2CH_2O^*$, $HOCH_2CHO^*$, and $OCH_2CH_2O^*$, undergo a greater reduction in free energy than $HOCH_2CH_2OH^*$, as there is only a weak dependence of the hydroxyl-metal interaction on atomic oxygen binding energy.[7] As a result, the free energy of reaction $HOCH_2CH_2OH^* \rightarrow HOCH_2CH_2O^* + H^*$ decreases, as does that of $HOCH_2CH_2O^* \rightarrow OCH_2CH_2O^* + H^*$ (that of $HOCH_2CH_2O^* \rightarrow HOCH_2CHO^* + H^*$ does not change as a function of O binding energy). BEP relationships indicate that this reduction in free energy of reaction lowers the reaction free energy barrier. This explains both the change in reaction path from Pt to Ni/Pt[8] and the increase in global reaction rate because of the increased rate of early dehydrogenation reactions. A substantial increase in O binding energy results in loss of selectivity because of C−O bond breaking reactions (deoxygenation), which form surface hydrocarbon fragments and O* (and other O bound adsorbates) that begin poisoning the surface. These deactivation mechanisms cause steep reduction in hydrogen production rates, as can be seen in the upper right portions of panels B and C of Figure 7. This finding agrees well with experimental evidence, as surfaces that bind oxygen and carbon more strongly, for instance the Co/Pt catalyst, have higher selectivity to C−O bond cleaving reactions.[62,64]

The other descriptors (H and C binding energy) also have interesting effects on the overall rate. As is well-known in oxygenate reforming, CO* acts as an inhibitor through site blocking. The free energy of CO* is directly proportional to the free energy of C*.[26] Thus, to improve the hydrogen production, the C binding energy should be lowered from its value on Pt. Lowering the C atomic binding energy significantly leads C−C bond breaking reactions to become rate limiting. This trade-off rationalizes the maximum observed in Figure 7(A−C) in the *y*-axes. An important implication for design of hydrodeoxygenation catalysts is that high selectivities to hydrocarbon products (albeit at lower activities because of high coverages) can be achieved at moderate C_{BE} (∼160−170 kcal/mol) and high O_{BE} (∼170 kcal/mol). This regime allows for C−O bond cleaving events to become much more active than C−C bond cleaving events.

Figure 7D illustrates the strong dependence of hydrogen production on the atomic binding energy of hydrogen. As the binding energy is increased, the free energy of dehydrogenation reactions decreases (assuming no adsorbates' free energy other than H* is affected by the H binding energy). This in turn will lower the kinetic barriers to dehydrogenation based on the BEP relationships used. However, increasing the H binding energy too far results in poisoning of the surface by H*. Jones et al. have shown that hydrogen binding energy has a linear correlation with carbon binding energy for certain systems.[29] This suggests that there is an optimal C binding energy that encompasses the effect of hydrogen binding energy. Unfortunately, it is difficult to design around hydrogen binding energy, as most single and bimetallic catalysts have hydrogen binding energies that fall within a tight window,[28] that is, the scatter in the linear (C and H) correlation can outweigh the usefulness of this particular correlation in the active regime.

The model predicts an increase in hydrogen production of more than an order of magnitude from Pt to Ni/Pt and another jump of greater than a factor of 2 to the optimal catalyst (Table 5). While the magnitude in rate increase is less in experiments,[11,72] it is important to remember that our model is idealistic in nature, and the actual supported catalyst may not be a single monolayer of Ni on Pt. This departure from idealistic models to real systems, along with the uncertainty in atomic binding energy descriptor models,[31] are important to keep in mind when using our results to predict effective polyol reforming catalysts. It should also be noted that implicit in this model is the assumption of a single catalyst site type. The development of multifunctional catalysts can also lead to increased activity or selectivity through the specific targeting of important elementary reactions to be favorably carried out on specific sites. This model, while of qualitative nature, is useful for screening out inactive catalysts and for identification of promising surfaces that justify the investment of time and resources on pursuing experimentally and with more expensive modeling techniques (as that of section 3).

5. CONCLUSIONS

Two detailed catalytic kinetic models were constructed to generate fundamental insights into the surface reaction mechanisms of ethylene glycol decomposition. The first model was parametrized using DFT and statistical mechanics calculations to describe this chemistry on Pt. This model confirmed that the primary pathway to decomposition is through initial O−H bond cleavage of ethylene glycol. However, as temperature increases, the pathway through initial C−H bond cleavage becomes more active. The model shows that unlike TPD experiments,[8] hydrogenation reactions (because of adequate surface coverages of H*) can facilitate the decomposition by opening up lower energy pathways. Further, reaction path analysis shows that C−C bond cleavage happens through several highly dehydrogenated intermediates: $HOCH_2CO^*$, $HOCHCO^*$, $OCCHO^*$, and $OCCO^*$. Sensitivity analysis shows that these C−C bond cleaving reactions are not rate determining. Rather, initial dehydrogenation reactions, specifically $HOCH_2CH_2O^* \rightarrow HOCH_2CHO^* + H^*$, are kinetically controlling. As seen in the semiempirical parametrized model, this has important ramifications for computational screening of catalysts.

The second model was parametrized based on atomic binding energy descriptors via linear scaling and BEP relationships derived both in literature and in this work. This model shows that an increase in atomic oxygen binding energy from 89 to 119 kcal/mol leads to the increased activity and rationalizes that the Ni/Pt catalyst is better than the Pt catalyst for this reaction because of increasing the initial dehydrogenation reaction rates. Further improvement to ethylene glycol reforming catalysts should center on maintaining this active regime of oxygen binding energies (∼115−120), while reducing the carbon binding energy slightly (∼145−150 kcal/mol), to reduce the coverage of CO* during steady state conditions. Finally, the model shows that the hydrogen production rates are sensitive to the hydrogen binding energy, and this descriptor needs to also be accounted for in a model. Further work should center on the development of stable, cost-effective catalysts that match the binding energy descriptors shown here. These models can greatly reduce the number of candidate materials that future experimental and high-level theoretical efforts should focus on.

■ ASSOCIATED CONTENT

Supporting Information. Calculated thermochemical properties of all intermediates on Pt(111), calculated thermochemical properties of the transition states used in the Pt model, a full list of reactions included in both models, graphs of the linear free energy relationships derived in this work, and more information on the correlations of adsorbate−adsorbate interaction used in both models, the linear scaling relationships used in the semiempirical model, and information on the choice of reactor design equation for both models. This material is available free of charge via the Internet at http://pubs.acs.org.

■ AUTHOR INFORMATION

Corresponding Author

*E-mail: vlachos@udel.edu. Phone: 302-831-2830.

Funding Sources

This material is based upon work financially supported as part of the Catalysis Center for Energy Innovation, an Energy Frontier Research Center funded by the U.S. Department of Energy, Office of Science, Office of Basic Energy Sciences under Award Number DE-SC0001004.

■ ACKNOWLEDGMENT

We thank Dr. Michail Stamatakis for helpful discussions. DFT calculations were performed using the TeraGrid resources provided by University of Illinois' National Center for Supercomputing Applications (NCSA).

■ REFERENCES

(1) Spath, P. L.; Dayton, D. C. *Preliminary Screening—Technical and Economic Assessment of Synthesis Gas to Fuels and Chemicals with Emphasis on the Potential for Biomass-Derived Syngas*; National Renewable Energy Laboratory: Golden, CO, 2003.
(2) Elliott, D. C. *Energy Fuels* **2007**, *21*, 1792.
(3) Dauenhauer, P. J.; Salge, J. R.; Schmidt, L. D. *J. Catal.* **2006**, *244*, 238.
(4) Davda, R. R.; Shabaker, J. W.; Huber, G. W.; Cortright, R. D.; Dumesic, J. A. *Appl. Catal., B* **2005**, *56*, 171.
(5) Griffin, M. B.; Jorgensen, E. L.; Medlin, J. W. *Surf. Sci.* **2010**, *604*, 1558.
(6) Kandoi, S.; Greeley, J.; Simonetti, D.; Shabaker, J.; Dumesic, J. A.; Mavrikakis, M. *J. Phys. Chem. C* **2011**, *115*, 961.
(7) Salciccioli, M.; Chen, Y.; Vlachos, D. G. *J. Phys. Chem. C* **2010**, *114*, 20155.
(8) Salciccioli, M.; Yu, W.; Barteau, M. A.; Chen, J. G.; Vlachos, D. G. *J. Am. Chem. Soc.* **2011**, *133*, 7996.
(9) Skoplyak, O.; Barteau, M. A.; Chen, J. G. *J. Phys. Chem. B* **2006**, *110*, 1686.
(10) Skoplyak, O.; Barteau, M. A.; Chen, J. G. *Surf. Sci.* **2008**, *602*, 3578.
(11) Stottlemyer, A. L.; Ren, H.; Chen, J. G. *Surf. Sci.* **2009**, *603*, 2630.
(12) Ji, N.; Zhang, T.; Zheng, M.; Wang, A.; Wang, H.; Wang, X.; Shu, Y.; Stottlemyer, A. L.; Chen, J. G. *Catal. Today* **2009**, *147*, 77.
(13) Ji, N.; Zhang, T.; Zheng, M. Y.; Wang, A. Q.; Wang, H.; Wang, X. D.; Chen, J. G. G. *Angew. Chem., Int. Ed.* **2008**, *47*, 8510.
(14) Gokhale, A. A.; Kandoi, S.; Greeley, J. P.; Mavrikakis, M.; Dumesic, J. A. *Chem. Eng. Sci.* **2004**, *59*, 4679.
(15) Salciccioli, M.; Stamatakis, M.; Caratzoulas, S.; Vlachos, D. G. *Chem. Eng. Sci.* **2011**, *66*, 4319.
(16) Blaylock, D. W.; Ogura, T.; Green, W. H.; Beran, G. J. O. *J. Phys. Chem. C* **2009**, *113*, 4898.
(17) Getman, R. B.; Schneider, W. F. *ChemCatChem* **2010**, *2*, 1450.
(18) Grabow, L. C.; Gokhale, A. A.; Evans, S. T.; Dumesic, J. A.; Mavrikakis, M. *J. Phys. Chem. C* **2008**, *112*, 4608.
(19) Kandoi, S.; Greeley, J.; Sanchez-Castillo, M. A.; Evans, S. T.; Gokhale, A. A.; Dumesic, J. A.; Mavrikakis, M. *Top. Catal.* **2006**, *37*, 17.
(20) Abild-Pedersen, F.; Greeley, J.; Studt, F.; Rossmeisl, J.; Munter, T. R.; Moses, P. G.; Skulason, E.; Bligaard, T.; Nørskov, J. K. *Phys. Rev. Lett.* **2007**, 99.
(21) Fernandez, E. M.; Moses, P. G.; Toftelund, A.; Hansen, H. A.; Martinez, J. I.; Abild-Pedersen, F.; Kleis, J.; Hinnemann, B.; Rossmeisl, J.; Bligaard, T.; Nørskov, J. K. *Angew. Chem., Int. Ed.* **2008**, *47*, 4683.
(22) Jones, G.; Bligaard, T.; Abild-Pedersen, F.; Nørskov, J. K. *J. Phys.: Condens. Matter* **2008**, 20.
(23) Shustorovich, E.; Sellers, H. *Surf. Sci. Rep.* **1998**, *31*, 5.
(24) Choi, Y.; Liu, P. *J. Am. Chem. Soc.* **2009**, *131*, 13054.
(25) Falsig, H.; Hvolbæk, B.; Kristensen, I. S.; Jiang, T.; Bligaard, T.; Christensen, C. H.; Nørskov, J. K. *Angew. Chem., Int. Ed.* **2008**, *47*, 4835.
(26) Ferrin, P.; Mavrikakis, M. *J. Am. Chem. Soc.* **2009**, *131*, 14381.
(27) Ferrin, P.; Simonetti, D.; Kandoi, S.; Kunkes, E.; Dumesic, J. A.; Nørskov, J. K.; Mavrikakis, M. *J. Am. Chem. Soc.* **2009**, *131*, 5809.
(28) Hansgen, D. A.; Vlachos, D. G.; Chen, J. G. G. *Nat. Chem.* **2010**, *2*, 484.
(29) Jones, G.; Jakobsen, J. G.; Shim, S. S.; Kleis, J.; Andersson, M. P.; Rossmeisl, J.; Abild-Pedersen, F.; Bligaard, T.; Helveg, S.; Hinnemann, B.; Rostrup-Nielsen, J. R.; Chorkendorff, I.; Sehested, J.; Nørskov, J. K. *J. Catal.* **2008**, *259*, 147.
(30) Schumacher, N.; Boisen, A.; Dahl, S.; Gokhale, A. A.; Kandoi, S.; Grabow, L. C.; Dumesic, J. A.; Mavrikakis, M.; Chorkendorff, I. *J. Catal.* **2005**, *229*, 265.
(31) Ulissi, Z.; Prasad, V.; Vlachos, D. G. *J. Catal.* **2011**, *281*, 339.
(32) Mhadeshwar, A. B.; Vlachos, D. G. *Catal. Today* **2005**, *105*, 162.
(33) Prasad, V.; Karim, A. M.; Arya, A.; Vlachos, D. G. *Ind. Eng. Chem. Res.* **2009**, *48*, 5255.
(34) Soler, J. M.; Artacho, E.; Gale, J. D.; Garcia, A.; Junquera, J.; Ordejon, P.; Sanchez-Portal, D. *J. Phys.: Condens. Matter* **2002**, *14*, 2745.
(35) Ordejón, P.; Artacho, E.; Soler, J. M. *Phys. Rev. B* **1996**, *53*, 10441.
(36) Troullier, N.; Martins, J. L. *Phys. Rev. B* **1991**, *43*, 8861.
(37) Perdew, J. P.; Burke, K.; Ernzerhof, M. *Phys. Rev. Lett.* **1996**, *77*, 3865.
(38) Chen, Y.; Vlachos, D. G. *J. Phys. Chem. C* **2010**, *114*, 4973.
(39) Reuter, K.; Scheffler, M. *Phys. Rev. B* **2002**, 65.
(40) Alcalá, R.; Mavrikakis, M.; Dumesic, J. A. *J. Catal.* **2003**, *218*, 178.
(41) Greeley, J.; Mavrikakis, M. *J. Am. Chem. Soc.* **2002**, *124*, 7193.
(42) Burgess, D. R. In *NIST Standard Reference Database Number 69*; Linstrom, P. J., Mallard, W. G., Eds.; National Institute of Standards and Technology: Gaithersburg, MD, 2009.
(43) ZumMallen, M. P.; Schmidt, L. D. *J. Catal.* **1996**, *161*, 230.
(44) Houston, P. L. *Chemical Kinetics and Reaction Dynamics*; Dover Publications, Inc.: Mineola, NY, 2001.
(45) Frenklach, M.; Wang, H.; Goldenberg, M.; Smith, G. P.; Golden, D. M.; Bowman, C. T.; Hanson, R. K.; Gardiner, W. C.; Lissianski, V.; *GRI-Mech, an optimized detailed chemical reaction mechanism for methane combustion*; Gas Research Institute: Chicago, IL, 1995.
(46) Mhadeshwar, A. B.; Vlachos, D. G. *Ind. Eng. Chem. Res.* **2007**, *46*, 5310.
(47) Yeo, Y. Y.; Vattuone, L.; King, D. A. *J. Chem. Phys.* **1997**, *106*, 392.
(48) Ludwig, J.; Vlachos, D. G. *J. Chem. Phys.* **2008**, 128.
(49) Ludwig, J.; Vlachos, D. G.; van Duin, A. C. T.; Goddard, W. A. *J. Phys. Chem. B* **2006**, *110*, 4274.
(50) Hansgen, D. A. University of Delaware, 2011.
(51) Wang, S. G.; Temel, B.; Shen, J. A.; Jones, G.; Grabow, L. C.; Studt, F.; Bligaard, T.; Abild-Pedersen, F.; Christensen, C. H.; Norskov, J. K. *Catal. Lett.* **2011**, *141*, 370.
(52) Li, M.; Guo, W. Y.; Jiang, R. B.; Zhao, L. M.; Shan, H. H. *Langmuir* **2009**, *26*, 1879.

(53) Michaelides, A.; Liu, Z. P.; Zhang, C. J.; Alavi, A.; King, D. A.; Hu, P. *J. Am. Chem. Soc.* **2003**, *125*, 3704.
(54) Mhadeshwar, A. B.; Kitchin, J. R.; Barteau, M. A.; Vlachos, D. G. *Catal. Lett.* **2004**, *96*, 13.
(55) Grabow, L. C.; Hvolbaek, B.; Norskov, J. K. *Top. Catal.* **2010**, *53*, 298.
(56) Podkolzin, S. G.; Alcala, R.; de Pablo, J. J.; Dumesic, J. A. *J. Phys. Chem. B* **2002**, *106*, 9604.
(57) Salciccioli, M.; Chen, Y.; Vlachos, D. G. *Ind. Eng. Chem. Res.* **2011**, *50*, 28.
(58) İnoğlu, N.; Kitchin, J. R. *Phys. Rev. B* **2010**, 82.
(59) Miller, S. D.; Kitchin, J. R. *Surf. Sci.* **2009**, *603*, 794.
(60) He, R.; Davda, R. R.; Dumesic, J. A. *J. Phys. Chem. B* **2005**, *109*, 2810.
(61) Skoplyak, O.; Barteau, M. A.; Chen, J. G. *Catal. Today* **2009**, *147*, 150.
(62) Skoplyak, O.; Menning, C. A.; Barteau, M. A.; Chen, J. G. *Top. Catal.* **2008**, *51*, 49.
(63) Greeley, J.; Mavrikakis, M. *J. Am. Chem. Soc.* **2004**, *126*, 3910.
(64) Skoplyak, O.; Menning, C. A.; Barteau, M. A.; Chen, J. G. *J. Chem. Phys.* **2007**, 127.
(65) Dougherty, E. P.; Rabitz, H. *J. Chem. Phys.* **1980**, *72*, 6571.
(66) Kramer, M. A.; Rabitz, H.; Calo, J. M.; Kee, R. J. *Int. J. Chem. Kinet.* **1984**, *16*, 559.
(67) Rabitz, H. *Comput. Chem.* **1981**, *5*, 167.
(68) Rabitz, H.; Kramer, M.; Dacol, D. *Annu. Rev. Phys. Chem.* **1983**, *34*, 419.
(69) Campbell, C. T. *Top. Catal.* **1994**, *1*, 353.
(70) Campbell, C. T. *J. Catal.* **2001**, *204*, 520.
(71) Shabaker, J. W.; Davda, R. R.; Huber, G. W.; Cortright, R. D.; Dumesic, J. A. *J. Catal.* **2003**, *215*, 344.
(72) Huber, G. W.; Shabaker, J. W.; Evans, S. T.; Dumesic, J. A. *Appl. Catal., B* **2006**, *62*, 226.